tributions in Supersonic and Hypersonic Flow," *AIAA Journal*, Vol. 1, No. 3, March 1963, pp. 634–639.

[7] Markovin, M. V., Donohoe, J. C., and Larson, H. K., "Exploratory Investigations of the Effects of Gas Injection Through a Porous Model on Separation, Transition, Static Stability, and Control Effectiveness of a Blunt Entry Body at Mach number 7.3," AIAA Paper 68-27, New York, 1968.

[8] Markovin, M. V. and Donohoe, J. C., "Exploratory Investigations of the Effects of Gas Injection Through a Porous Model on Separation, Transition, Static Stability, and Control Effectiveness of a Blunt Entry Body at Mach number 7.3," Rept. ER 14598, Contract NAS 2-3873, July 1967, Martin Marietta Corp.

[9] Keyes, J. W. and Ashley, G. C., Jr., "Calculated and Experimental Hinge Moments on a Trailing-Edge Flap of a 75 Swept Delta Wing at Mach 6," TND-4268, Dec. 1967, NASA.

[10] Ericsson, L. E. and Reding, J. P., "Aerodynamic Effects of Bulbous Bases," CR-1339, Aug. 1969, NASA.

[11] Rainbird, W. J., "Turbulent Boundary-Layer Growth and Separation on a Yawed Cone," *AIAA Journal*, Vol. 6, No. 12, Dec. 1968, pp. 2410–2416.

[12] Tobak, M., Schiff, L. B., and Peterson, V. L., "Aerodynamics of Bodies of Revolution in Non-planar Motion," AIAA Paper 68-20, New York, 1968.

[13] Schiff, L. B., "A New Wind Tunnel Apparatus for Studying Coning and Spinning Motions of Bodies of Revolution," *Proceedings of the 3rd Technical Workshop on Dynamic Stability Problems*, NASA Ames Research Center, Nov. 1968.

[14] Maikapar, G. I., "Aerodynamic Heating of the Lifting Bodies," paper RE126, Oct. 1968, XIXth Congress of the International Astronautical Federation, New York.

[15] Edny, B., "Anomalous Heat Transfer and Pressure Distributions on Blunt Bodies at Hypersonic Speeds in the Presence of an Impinging Shock," FFA Rept. 115, Feb. 1968, The Aeronautical Research Institute of Sweden.

FEBRUARY 1970 J. SPACECRAFT VOL. 7, NO. 2

Flight Test Measurements of Boundary-Layer Transition on a Nonablating 22° Cone

M. M. SHERMAN* AND T. NAKAMURA†
Philco-Ford Corporation, Newport Beach, Calif.

Boundary-layer transition measurements were obtained on four flight tests of an experimental re-entry vehicle. The vehicle was a sharp, 22° half-angle cone with a beryllium heatshield and a graphite nose tip. Thermocouples and pressure taps were located on the cone surface and aft cover. Telemetered data were clear and consistent from flight to flight. The measured temperature histories agreed with preflight predictions during the period of laminar flow, and boundary-layer transition was clearly observed on all of the sensors. The transition process consisted of transitional flow which moved forward along the surface at a relatively fast rate, followed by the sudden occurrence of fully turbulent flow over the entire vehicle. The base temperature and pressure measurements verified the cone surface transition events. However, the base to freestream pressure ratios recorded during turbulent flow were significantly higher than have previously been reported for flight tests of more slender re-entry vehicles.

Nomenclature

C_f = local skin-friction coefficient
h = enthalpy
Re_X = Reynolds number based on wetted length
Re_θ = Reynolds number based on boundary-layer momentum thickness
u = velocity
x = surface distance
ρ = gas density

Subscripts

e = edge of boundary layer
r = recovery
w = wall

Introduction

PREFLIGHT predictions of boundary-layer transition are important to the design of many re-entry vehicles. As a result, many theoretical and experimental studies of this subject have been performed in recent years.[1–7] The objective of most of these experimental programs is to isolate and evaluate the effects of the many individual parameters that are known to influence transition. However, interpretation of these ground-test data is complicated by the fact that conditions associated with the test facility operation may also influence the transition process. The extent and magnitude of these effects are not always known. Therefore, controlled flight test measurements are the most desirable means of obtaining transition data, and offer the additional advantage of permitting evaluation of the more easily obtained ground-test results.

Most re-entry vehicles are designed for high performance flight and must necessarily use ablative heatshields. These vehicles sometimes contain instrumentation from which it is possible to obtain useful measurements of boundary-layer transition. Unfortunately, the effects of mass injection from the ablating surface cannot be uncoupled from these flight results. For purposes of obtaining a more basic understanding of the transition phenomena, it is desirable to obtain direct flight test measurements in the absence of mass transfer.

The present flight test program employed four identical conical vehicles with nonablating heatshields. These vehicles were instrumented to obtain accurate measurements of the cone surface temperature histories at several axial locations,

Presented as Paper 68-1152 at the AIAA Vehicle Systems and Technology Meeting, Williamsburg, Va., December 3–5, 1968; submitted February 6, 1969; revision received October 13, 1969.

* Supervisor, Thermodynamics Unit, Space and Re-Entry Systems Division. Member AIAA.

† Senior Engineering Specialist, Space and Re-Entry Systems Division.

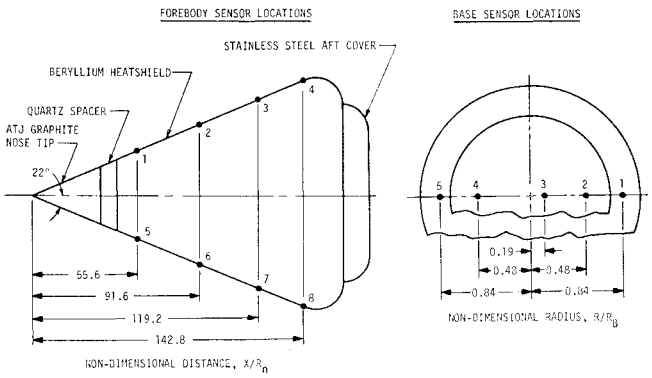

Fig. 1 External vehicle profile and sensor locations.

in addition to other temperature and pressure measurements. These data provided clear and consistent histories of the progression of boundary-layer transition over the surface of the vehicles.

Vehicle Description and Performance

The re-entry vehicle used in the flight test program was a 22° half-angle cone with a homogeneous ATJ graphite nose tip, followed by a 1.8-in.-long quartz spacer. The main body heatshield was beryllium and the base cover was stainless steel. Figure 1 is a sketch of the external vehicle profile showing the location of the thermal instrumentation. On the conical forebody, the instrumentation consisted of two longitudinal rows, 180° apart, of four thermocouples and adjacent pressure taps. The base cover contained five thermocouples and adjacent pressure taps at the three indicated radial locations. The base thermocouples were bonded to the inner surface of the 0.125 in. thick stainless steel cover.

The four vehicles were all flown on identical trajectories. The only significant difference in the four flights concerned the initial angle-of-attack and spin rate of the fourth vehicle. This last vehicle was intentionally injected at a large angle of attack; however, a failure in the attitude control system

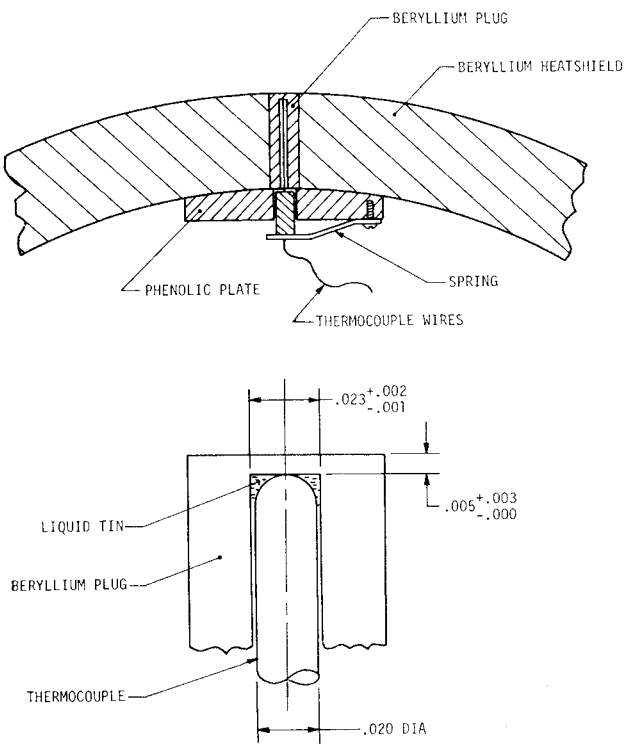

Fig. 2 Heatshield thermocouple installation.

Table 1 Entry flight parameters

Flight No.	1	2	3	4
α_i (deg)	8.6	1.25	2.6	48.2
α_f (deg)	<1	<1	<1	~2
ω_i (rpm)	30.5	20.7	29.3	1.1

prevented spin-up to the desired rate. Table 1 summarizes the initial angle-of-attack (α_i) and spin rate ($\dot{\omega}_i$) for the four flights, along with the angle-of-attack at 100 kft (α_f) for use in later discussions.

On-Board Instrumentation

The primary transition measurements were obtained by means of the eight surface temperature thermocouples on the conical forebody. Figure 2 shows the installation of these thermocouples in the beryllium heatshield. The cone sensors were all Type K (chromel-alumel) thermocouples with a grounded junction enclosed in a 0.020-in.-diam stainless steel sheath. The thermocouple assembly was spring-loaded to hold the junction against the end of the 0.023 in. (nominal) diameter cavity.

The presence of the thermocouple cavity in the heatshield creates a local hot spot such that the undisturbed temperature exists at some distance below the surface. The cavity dimensions were selected, according to the methods described by Beck and Hurwicz,[8] to permit the embedded thermocouple to sense the undisturbed heatshield surface temperature within prespecified limits of ±70°F.

Good thermal contact between the thermocouple tip and the metal surface was assured by the addition of a short (0.030 in.) slug of 0.020-in.-diam pure tin wire between the thermocouple and the bottom of the cavity. Calculations showed that the maximum error in the measured surface temperature caused by the solid tin slug would be 15° to 20°F, and that the tin would melt during re-entry at an altitude of around 120 kft, or at the upper end of the expected transition altitude range. Also, very small temperature increases cause the tin to soften and deform under the spring load, providing improved thermal contact. After the tin melts, the spring force on the sheath pushes the thermocouple tip against the bottom of the cavity. The flight deceleration and centrifugal forces keep the liquid tin at the end of the cavity surrounding the sheath, thereby maintaining the desired wetted metallic contact.

Calculations were performed to estimate the errors in the surface temperature measurement associated with the embedded thermocouple configuration. Using the results of Ref. 8, the errors were determined for two cases, corresponding to the nominal and extreme cavity dimensions. For these calculations, an average thermal conductivity of the beryllium of 72 Btu/ft-hr-°F was assumed. The effect of the presence of the thermocouple sheath and liquid tin was included by assuming an average thermal conductivity for the cavity composite of 25 Btu/ft-hr-°F.

The computed error for constant, or slowly varying, heating, i.e., laminar flow, is illustrated in Fig. 3a for the nominal and maximum cases. The error is seen to be less than 20°F for heating rates up to 600 Btu/ft²-sec, which is greater than the maximum laminar heating rate experienced during the entry trajectory. The response of the thermocouple to sudden changes in heating rate, i.e., transition, was investigated by computing the transient temperature response at the bottom of the cavity following a step change in surface heat flux of 1000 Btu/ft²-sec. As shown in Fig. 3b, the temperature at the thermocouple location (T_M) is within 10°F of the undisturbed surface temperature (T_0) in less than 3 msec. Thus, the flight thermocouple installation was deemed to be satisfactory for the measurement of the heat-

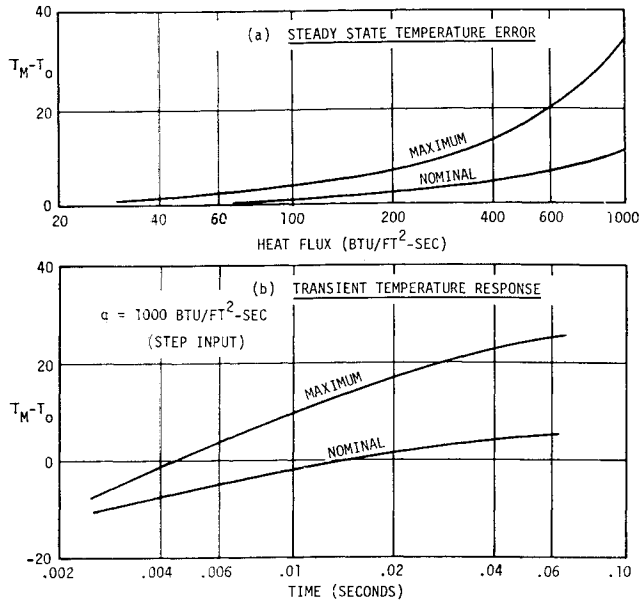

Fig. 3 Computed thermocouple characteristics.

shield surface temperature history and the detection of boundary layer transition.

All of the cone surface and base cover thermocouples had a full-scale range of 0° to 2250°F. Sampling rates of 80 samples/sec (sps) and 20 sps were used for the cone and base thermocouples, respectively. Base pressure sensor 1, 3, and 5 (Fig. 1) had ranges of 0 to 0.1 psia, while sensor 2 and 4 were sized for 0 to 1.0 psia. The base pressures were monitored at 40 sps.

Other on-board instrumentation which was used to detect or confirm boundary-layer transition included: 1) A three-axis inertial reference unit which measured the pitch, yaw, and roll attitude of the vehicle. The attitude sensors had ranges of ±11.25° and were sampled at 80 sps. 2) Three longitudinal accelerometers with ranges of 0.8, 6.0, and 16 g's, respectively. The high range (16 g) accelerometer was monitored at 320 sps, and the other two accelerometers at 160 sps.

Flight Test Data

Data were received from a total of 30 of the 32 possible cone temperature sensors, 19 of the 20 base temperatures, and 16 of the 20 base pressure sensors on the four flights. Figures 4–6 are typical plots of each of these measurements. The plots have been enlarged to encompass the altitude range over which transition occurred.

The measured cone surface temperature histories, e.g., Fig. 4, increased at the same rate as the preflight laminar heating predictions until the onset of transition. Many of the cone surface temperatures were slightly biased from the assumed surface temperature at the beginning of re-entry. These displacements were variable in magnitude and are attributed to calibration errors.

Transition on the conical surface was observed to occur in two distinct phases. The first phase was transitional flow, which is seen to begin at an altitude of 110 kft in Fig. 4, and is characterized by surface temperature rise rates of approximately 500 to 1500°F/sec, dependent on the body station. Following this, fully turbulent flow occurred 6 to 10 kft later (at 99 and 100 kft in Fig. 4), and this phase was characterized by surface temperature rise rates of 2000 to 5000°F/sec. The onset of fully turbulent flow was not observed on some of the aft sensors since their longer period of exposure to transitional flow heating resulted in instrument saturation (2250°F) before transition was completed. Also,

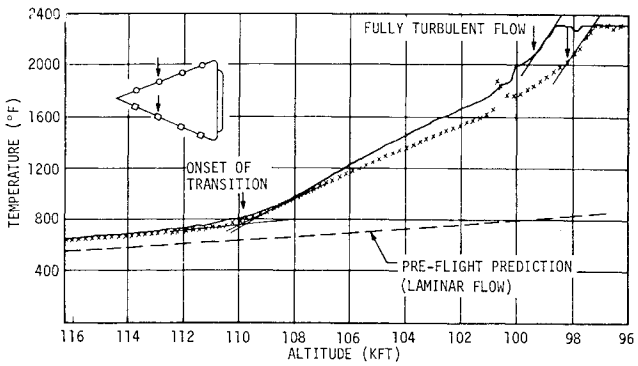

Fig. 4 Typical cone surface temperature histories.

the measured change in surface temperature during turbulent flow is seen to be much smaller than that which occurs in the transitional period (due to the 2250°F limit); and this results in some uncertainty in the interpretation of the recorded data. However, the temperature rise rates which have been derived from the fully turbulent flow portions of the temperature histories have been found to agree quite closely with the theoretical values for turbulent heating.

The base pressure histories (Fig. 5) experience a small pressure pulse (or dip) at altitudes roughly corresponding to the onset of transitional flow on the conical surface, while the base temperature histories (Fig. 6) do not exhibit any detectable change during this period. However, both the base temperature and pressure histories exhibit marked increases at the same time as the establishment of fully turbulent flow on the cone.

Figure 5 also includes the preflight laminar and turbulent flow base pressure predictions. The laminar flow predictions were based on the data of Baum, King, and Denison,[9] while the turbulent flow predictions were based on the data of Cassanto.[10] Good agreement is seen for both cases. Cassanto's data, which show the base pressure as a function of the cone pressure and Mach number, were obtained for the same local Mach number range experienced by this vehicle, but for much smaller cone angles and freestream Mach numbers. Figure 7 shows the recorded base pressure history as the ratio of base to freestream pressure. These recorded turbulent flow base pressure histories are significantly higher than have previously been reported for flight tests of more slender re-entry vehicles.

Gross or indirect indications of boundary-layer transition were also obtained from other on-board and remote sensors.

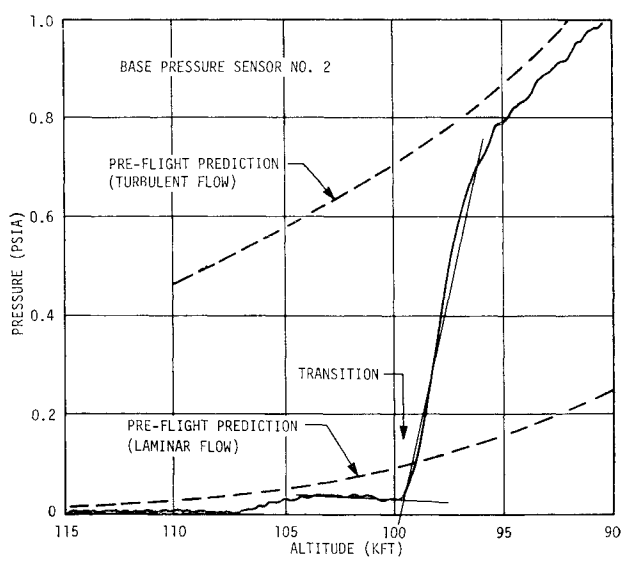

Fig. 5 Typical base pressure history.

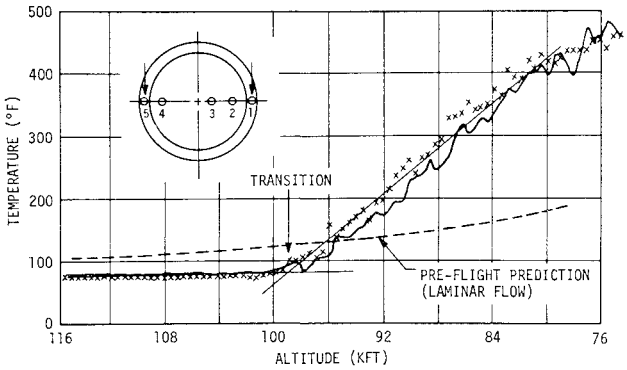

Fig. 6 Typical base temperature histories.

These measurements, which are summarized in Fig. 8 along with the primary data sources, are listed below.

1) Two slope changes were noted in the axial acceleration histories. The first, and smaller, change corresponds approximately to the onset of transitional flow as detected by the cone surface temperature sensors. The time of the second, more definite slope change agrees very closely with the beginning of fully turbulent flow on the cone.

2) The yaw and pitch attitude histories both exhibited changes in their oscillation frequency and magnitude at the time of fully turbulent flow.

3) The measured cone pressure histories, in many cases, exhibited small fluctuations and an apparent decrease in pressure just prior to the detection of surface melt by the heatshield surface temperature thermocouples. This is attributed to the localized melting of beryllium on the lip of the pressure ports. As such, these data provide an independent check on the beryllium melt altitude which immediately follows turbulent flow.

4) Beryllium melt was also detected both by radar (sudden increase in wake cross section) and optical (spectrographic) means at times corresponding to the beginning of the turbulent flow period. This is slightly earlier than the onset of general heatshield surface melting as detected by the surface temperature thermocouples, and may correspond to the melting of small localized areas such as the pressure ports.

Figure 8 graphically illustrates the good agreement between the various indicators of boundary-layer transition used in this flight test program. The consistency of results from the four flights is also apparent. These secondary on-board and remote transition measurements are considered to provide

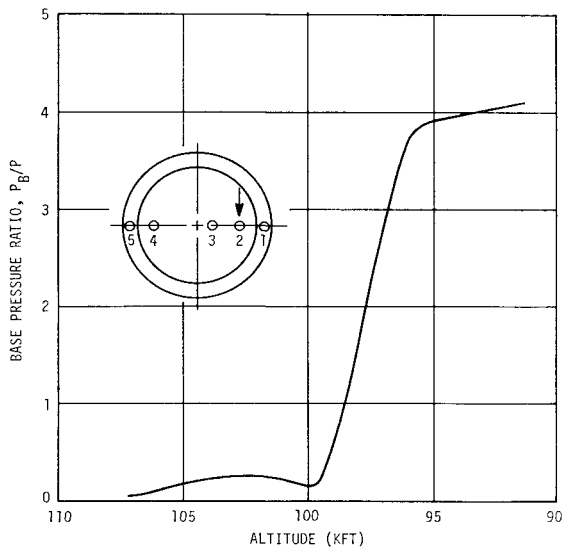

Fig. 7 Base pressure ratio history.

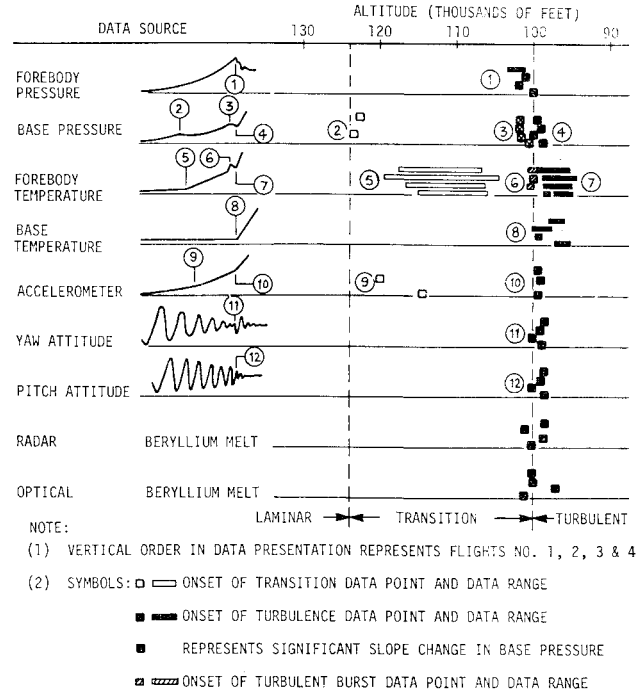

Fig. 8 Vehicle transition measurement summary.

gross verification of the detailed picture of the transition history which was obtained by means of the forebody surface temperature measurements.

Data Analysis

A postflight data analysis was performed to correlate the measured transition altitudes with the local inviscid flow conditions during the period of interest. The parameters of most importance were the local Mach number and Reynolds numbers based on both boundary-layer momentum thickness and wetted length. Because of the agreement between the slopes of the predicted and measured surface temperature histories, it was considered that an accurate representation of the local heat transfer and, therefore, skin-friction coefficient (C_f) histories was available. The laminar boundary-layer momentum thickness (θ) was then computed from the momentum integral equation without mass transfer or longitudinal pressure gradient,

$$d\theta/dx + \theta/x = C_f/2 \tag{1}$$

which is solved to give,

$$\theta/x = C_f/3 \tag{2}$$

The mass addition from the graphite nose tip during laminar flow is small compared to the local inviscid mass flow rate and will not significantly affect the above expression. The local skin friction coefficient was obtained from the

Table 2 Local Mach number and temperature ratio histories

Altitude (kft)	Mc	Temperature Ratio (T_w/T_r) at Axial Sensor Location No. 1	2	3	4
120	6.3	0.10	0.09	0.08	0.08
115	6.2	0.11	0.09	0.09	0.09
110	6.2	0.11	0.10	0.11	0.12
105	6.1	0.13	0.15	0.15	0.15
100	6.1	0.19	0.19	0.19	0.18
95	6.1	0.23	0.23	0.23	0.22
90	6.0	0.23	0.23	0.23	0.23

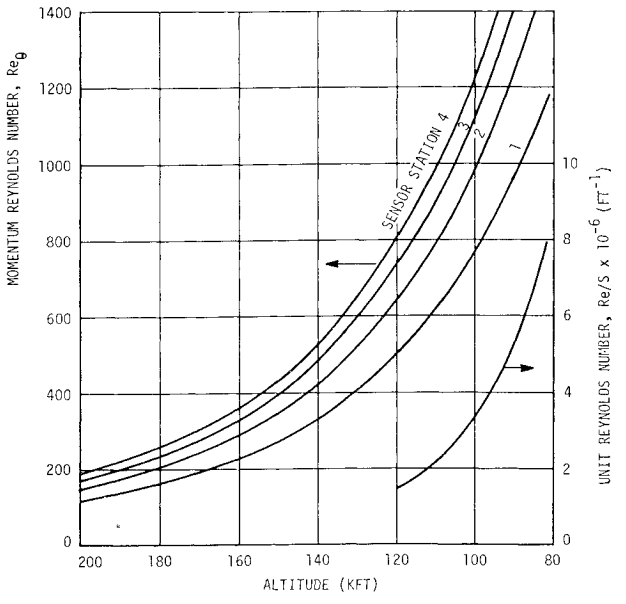

Fig. 9 Reynolds number histories.

reference enthalpy modification to the Blasius expression,

$$C_f = 0.664(\rho^*\mu^*/\rho_e\mu_e)^{1/2}/(R_{ex}/3)^{1/2} \quad (3)$$

with the starred quantities evaluated at the reference enthalpy (h*),

$$h^* = 0.5(h_w - h_e) + 0.22\,(h_r - h_e) \quad (4)$$

The wall enthalpy, h_w was based on the preflight predictions for laminar flow, and the local inviscid flow conditions were computed from real gas, sharp cone relationships. The validity of the sharp cone assumption was checked by performing a streamtube mass balance calculation to account for the effects of nose bluntness on the local inviscid flow. The results showed that, for this small nose radius and large cone angle, the entropy gradient region is swallowed on the nose tip and the sharp cone assumption is accurate for the entire heatshield surface. The computed laminar momentum thickness Reynolds number histories for the four cone sensor locations are shown in Fig. 9. Also included in Fig. 9 is the local Reynolds number per unit length, which is invariant along the surface because of the sharp cone flow field.

The local Mach number and the approximate ratio of the measured wall temperature (which was essentially the same for all flights) to the recovery temperature at the four sensor locations were as shown in Table 2 over the altitude range corresponding to the beginning of transitional and fully turbulent flow. All of the recorded surface temperature histories were examined in detail, and the onset of transitional flow and establishment of fully turbulent flow were defined at each sensor location (see Fig. 4). These results are shown in Fig. 10. As indicated, the total spread is small and the results are consistent from flight to flight. The results of Flight 4 (which entered with an initial angle of attack of 48°), are indistinguishable from the three preceding flights. However, a definite conclusion cannot be reached regarding the effects of angle of attack because of the sensor orientation during the transition period. The two sensor rows, which were 180° apart, were oriented such that the local angle of attack was small, i.e., they were between the windward and leeward rays. The spin rate for this flight (1 rpm) was such that the vehicle rotated only about 20° during the 30 kft descent which encompassed the entire transition period.

The transition altitude data of Fig. 10 were combined with the Reynolds number histories of Fig. 9 to obtain the corresponding curves for the laminar momentum thickness and

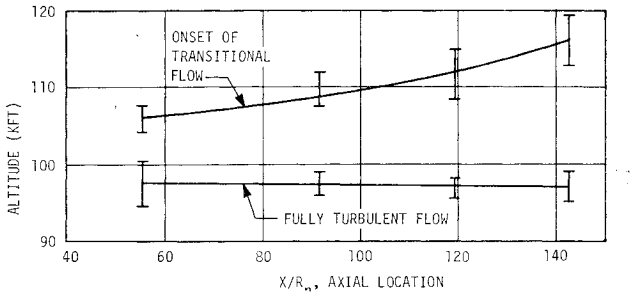

Fig. 10 Transition altitude vs axial location.

length Reynolds numbers for transitional and turbulent flow. These data are shown in Fig. 11.

The results indicate that transitional flow began at the aft end of the vehicle and moved forward along the conical surface at a decreasing (i.e., non-constant) value of the local Reynolds number. Fully turbulent flow then seemed to flash over the entire surface at once. (Therefore, the "fully turbulent flow" curves in Fig. 11 simply represent the local Reynolds number distributions over the surface at the time of transition.) It was not possible to determine, from detailed examination of the temperature histories of individual pairs or rows of sensors, whether turbulent flow occurred first at the forward or aft end of the vehicle. The transition to fully turbulent flow may have been induced (tripped) by small roughness elements on the ablating graphite nose tip or by the small gap between the quartz spacer and the beryllium heatshield.

Conclusions

Detailed measurements of boundary layer transition were obtained from four flight tests of a sharp, non-ablating, conical (22° half-angle) re-entry vehicle. The measurements were obtained by means of surface temperature histories of the beryllium heatshield. Transition was observed to occur in two distinct phases, which were: 1) a transitional flow characterized by surface temperature rise rates intermediate between the theoretical laminar and turbulent values, and 2) fully turbulent flow with surface temperature rise rates in agreement with turbulent flow predictions.

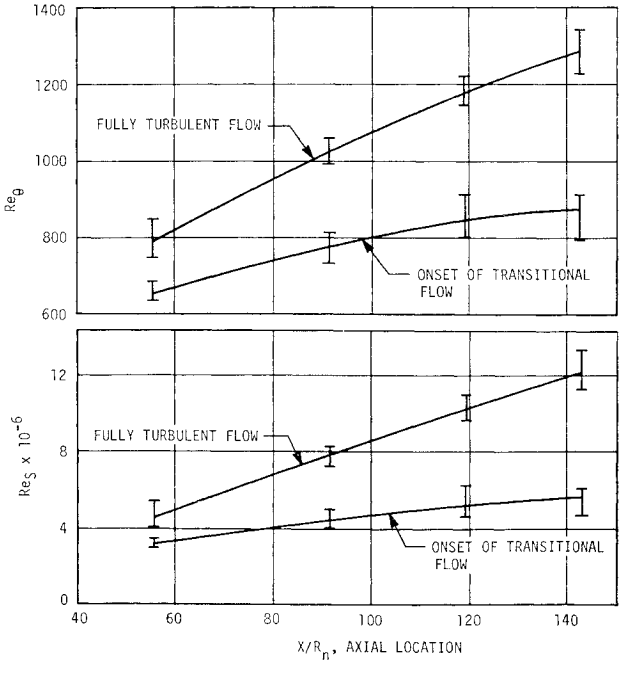

Fig. 11 Transition Reynolds number vs axial location.

Table 3 Transition measurement summary

Sensor Locations	Transitional flow		Turbulent flow	
	1 and 5	4 and 8	1 and 5	4 and 8
Altitude (kft)	106 ± 2	116 ± 4	97 ± 3	97 ± 2
Momentum Reynolds No., Re_θ	660 ± 30	850 ± 60	800 ± 50	1280 ± 60
Length Reynolds No., $Re_x \times 10^{-6}$	3.2 ± 0.2	5.3 ± 0.7	4.7 ± 0.7	12.2 ± 1.0

The transitional flow began at the aft end of the vehicle at an altitude of 116 ± 4 kft and progressed forward along the surface at a decreasing value of local Reynolds number. The establishment of fully turbulent flow occurred on all vehicles at an altitude of 97 ± 3 kft and appeared to flash simultaneously over the entire vehicle surface and base region. The occurrence of turbulent flow was verified with good agreement by several independent sensors and remote measurements. Table 3 summarizes the observed transition altitude and Reynolds number ranges at the forward and aft cone sensor locations for the four flights.

The base cover temperature histories did not experience any detectable change during the period of transitional flow on the cone, but showed a sudden change in slope at the time of fully turbulent cone flow. The measured base pressure histories exhibited a small pulsation at the start of transitional flow, followed by a sudden large increase at the time of fully turbulent cone flow. The recorded base pressure during turbulent flow was approximately four times the freestream pressure, which represents a higher base pressure ratio than has previously been reported.

References

[1] Stetson, K. F. and Rushton, G. H., "Shock Tunnel Investigation of Boundary-Layer Transition at $M = 5.5$," *AIAA Journal*, Vol. 5, No. 5, May 1967, pp. 899–906.

[2] Deem, R. E. and Murphy, J. S., "Flat Plate Boundary-Layer Transition at Hypersonic Speeds," AIAA Paper 65-128, New York, 1965.

[3] Nagamatsu, H. T. and Sheer, R. E., "Boundary-Layer Transition on a Highly Cooled 10° Cone in Hypersonic Flows," *Proceedings of AIAA Entry Technology Conference*, Williamsburg, Va., Oct. 1964, pp. 136–157.

[4] Potter, J. L. and Whitfield, J. D., "Effects of Slight Nose Bluntness and Roughness on Boundary Layer Transition in Supersonic Flows," *Journal of Fluid Mechanics* Vol. 12, 1962, pp. 508–535.

[5] White, C. O., "Boundary-Layer Transition for Sharp and Slightly Blunted Cones Under Hypersonic Entry Conditions," Rept. METN 110, Philco-Ford Corp., Space and Re-Entry Systems Div., Oct. 1966.

[6] Morkovin, M., "Critical Evaluation of Transition from Laminar to Turbulent Shear Layers with Emphasis on Hypersonically Traveling Bodies," AFFDL-TR-68-149, March 1969, Air Force Flight Dynamics Lab.

[7] Sanator, R. J., DeCarlo, J. P. and Torrillo, D. T., "Hypersonic Boundary-Layer Transition Data for A Cold Wall Slender Cone," *AIAA Journal*, Vol. 3, No. 4, April 1965, pp. 758–759.

[8] Beck, J. V. and Hurwicz, H., "Effect of Thermocouple Cavity on Heat Sink Temperature," *Journal of Heat Transfer*, Feb. 1969, pp. 27–36.

[9] Baum, E., King, H. H., and Denison, M. R., "Recent Studies of the Laminar Base-Flow Region," *AIAA Journal*, Vol. 2, No. 9, Sept. 1964, pp. 1527–1534.

[10] Cassanto, J. M., "Ratio on Base Pressure," *AIAA Journal*, Vol. 3, No. 12, Dec. 1965, p. 2351.